AIAA JOURNAL
Vol. 46, No. 7, July 2008

Noise-Source Identification for Ducted Fan Systems

Gareth J. Bennett* and John A. Fitzpatrick†
Trinity College Dublin,
Dublin 2, Ireland

DOI: 10.2514/1.33522

Coherence-based source analysis techniques can be used to identify the contribution of combustion noise in the exhaust of a jet engine and to hence enable the design of noise-reduction devices. However, when the combustion noise propagates in a nonlinear fashion, the identified contribution using ordinary coherence methods will be inaccurate. In this paper, an analysis technique is reported that enables the contribution of linear and nonlinear mechanisms to the propagated sound to be identified. An experimental rig is described for studying the propagation of noise through a rotor/stator setup using a vane axial fan mounted in a duct so that nonlinear interactions between a sound source and the fan can be investigated. The reported technique is used to identify a nonlinear tone generated by the interaction of the rotor and a propagated tone. The identification procedures are then applied to data from full-scale turbofan engine tests instrumented with pressure transducers at the combustor can and in the hot-jet pipe with microphones in the near field. At a particular power setting, the interaction between the combustion noise and the high-pressure turbine is measured in the hot-jet pipe. The analysis techniques enable nonlinear interactions to be identified and enable linear and nonlinear coherent output powers to be determined.

Nomenclature

$A_{m,n}(x)$	=	amplitude of the (m, n)th mode
C	=	combustor
F	=	fan
f	=	frequency, Hz
f_c	=	upper-frequency limit, Hz
f_{samp}	=	sample rate, samples per second, Hz
$G_{xx}(f)$	=	autospectral density function of $x(t)$
$G_{xy}(f)$	=	cross-spectral density function of $x(t)$ and $y(t)$
$H(f)$	=	frequency-response function
J_m	=	Bessel function of the first kind of order m
$k_{r,m,n}$	=	transverse eigenvalue of the (m, n)th mode, transverse wave number
M	=	Mach number
$\pm m$	=	azimuthal mode order in the shaft and countershaft directions, respectively.
N_p	=	number of data points per segment
n	=	radial mode order
$n(t)$	=	extraneous noise
$p(t)$	=	pressure signal
$\mathbf{Re}[\,]$	=	real part
RP$[1, 2, B]$	=	rumble probe 1, 2, B
T	=	turbine
$T_d(i)$	=	record length of segment i
Δf	=	frequency resolution, $1/T_d$, Hz
Δt	=	sampling resolution, $1/f_{\text{samp}}$, s
$\gamma^2_{xy}(f)$	=	ordinary coherence function of $x(t)$ and $y(t)$
$\Psi_{m,n}(r, \theta)$	=	eigenfunction of the (m, n)th mode
ω	=	frequency, $2\pi f$, rad/s
:	=	correlated part
·	=	conditioned or uncorrelated part

Subscripts

comb	=	combustion
down	=	downstream
exit	=	exit plane of an aeroengine, location in the hot-jet pipe
up	=	upstream

Superscripts

+	=	incident
−	=	reflected

I. Introduction

THE reduction of the two principal sources of aeroengine noise, the fan and the jet, has resulted in a new noise floor being reached. This will limit the benefits to be gained by further reducing these dominant components, unless the noise sources that set this threshold are in turn reduced. Of these, combustion, or core noise, which is considered here to be the sum of combustion and turbine noise, is an area of current research activity. At relatively low jet velocities (such as those that occur at engine idle, during taxiing, and at approach and cruise conditions), core noise is considered to be a significant contributor to the overall sound level. It will continue to receive attention, because the current trend toward high-bypass engines (which tend to reduce jet noise) and low-NO_x combustors (which may modify the noise characteristics) will result in core noise becoming a more significant source.

An acoustic measurement of a system of interest will most often be the summation of a number of separate acoustic sources, along with some extraneous noise. For the case in which it is not possible to remove individual sources without affecting the behavior of the others, the challenge is to decompose the measurement signal into its constituent parts. For acoustic sources that are considered to be stationary random processes with zero mean and in which systems are constant-parameter linear systems (Fig. 1), a multiple-input/single-output model can be used to represent the system. The extraneous noise term $n(t)$ accommodates all deviations from the model, such as additional acoustic sources that are unaccounted for. These deviations from the model can be a result of nonlinear operations, nonstationary effects, acquisition, and instrument noise, along with unsteady pressure fluctuations local to the sensor, such as flow or hydrodynamic noise. Because the many acoustic noise sources in an aeroengine overlap in the frequency domain, with

Presented as Paper 3693 at the 13th AIAA/CEAS Aeroacoustics Conference, Rome, Italy, 21–23 May 2007; received 17 July 2007; revision received 18 January 2008; accepted for publication 7 February 2008.

*Lecturer, Department of Mechanical and Manufacturing Engineering.
†Professor, Department of Mechanical and Manufacturing Engineering, Head of School.

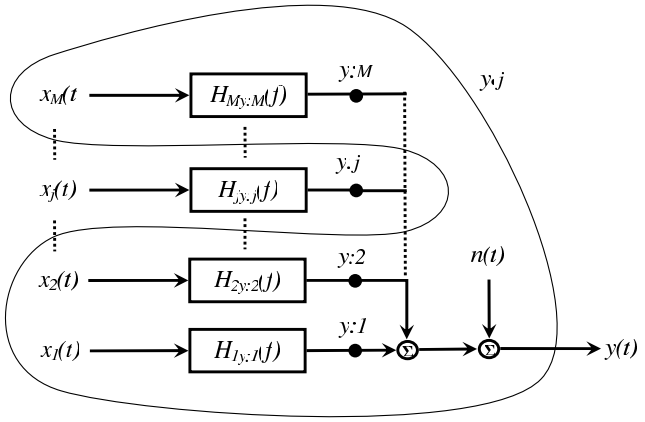

Fig. 1 Multiple-source acoustic measurement.

varying amplitudes, it can be difficult to quantify the individual contributions.

Coherence-based noise-source identification techniques can be used to identify the contribution of combustion noise to near- and far-field acoustic measurements of aeroengines. Karchmer and Reshotko [1], Karchmer et al. [2], and Reshotko and Karchmer [3] used the ordinary coherence function between internal measurements and far-field microphones and derived the core noise at far-field locations by calculating the coherent output power (COP): a technique reported initially by Halvorsen and Bendat [4]. Karchmer [5] also used the conditioned coherency function to determine where the source region for core noise was located. Extraneous noise contamination at an internal microphone location can result in the derived core noise at the far-field location being significantly lower than the true value. For such situations, Shivashankara [6,7] used Chung's [8] flow-noise-rejection technique to identify the internal core-noise contribution to far-field noise measurements. Hsu and Ahuja [9] extended Chung's [8] technique to develop a partial-coherence-based technique that uses five microphones to extract ejector internal mixing noise from far-field signatures that were assumed to contain the ejector mixing noise, the externally generated mixing noise, and also another correlated mixing noise, presumably from the ejector inlet. Whenever there is more than one source, all of these approaches necessitate the location of at least one sensor near one of the sources (e.g., the core-noise source) to measure that source in isolation. When there is only one source in the presence of extraneous noise, it has been shown that no direct measure of the source is necessary when using Chung's [8] technique. Minami and Ahuja [10] discussed a technique in which only far-field measurements are needed to separate any number of correlated sources from extraneous noise (which, due to its distributed nature, could be jet noise, for example). Previously published work in this area from the 1970s and 1980s has been revisited in more recent years by Hsu and Ahuja [9]. Bennett and Fitzpatrick [11] evaluated techniques that can be used to identify the contribution of combustion noise to near- and far-field acoustic measurements of aeroengines.

The preceding coherence-based source analysis techniques can be used to identify the contribution of combustion noise in the exhaust of a jet engine and hence to enable the design of noise-reduction devices. However, when the combustion noise propagates in a nonlinear fashion, the identified contribution using ordinary coherence methods will be inaccurate. In this paper, an analysis technique to enable the contribution of linear and nonlinear mechanisms to the propagated sound to be identified is reported. The technique is then applied to data from a small-scale rig and to data from full-scale turbofan engine tests.

II. Nonlinear Analysis

The coherence function $\gamma_{xy}^2(f)$ of two quantities $x(t)$ and $y(t)$ is the ratio of the square of the absolute value of the cross-spectral density function to the product of the autospectral density functions of the two quantities:

$$\gamma_{xy}^2(f) = \frac{|G_{xy}(f)|^2}{G_{xx}(f)G_{yy}(f)} \tag{1}$$

For all f, the quantity $\gamma_{xy}^2(f)$ satisfies $0 \le \gamma_{xy}^2(f) \le 1$.

As discussed by Bendat and Piersol [12] (p. 172, for example), the situation in which the coherence function is greater than zero but less than unity may be explained by one of the following three possible physical situations:

1) Extraneous noise is present in the measurements.
2) The system relating $x(t)$ and $y(t)$ is not linear.
3) The output $y(t)$ is due to an input $x(t)$ as well as to other inputs.

The underlying assumption with the identification techniques reviewed by Bennett and Fitzpatrick [11] is that the propagation path, from upstream of the turbine to a downstream measurement point, is linear. That is to say, to assume that a decrease in coherence is to be attributable to only the first and third of the preceding situations is to ignore the possibility of a nonlinear system.

A drop in coherence between combustion-noise measurements made at the combustor can with pressure transducers and microphone array measurements focused on the exit plane of an aeroengine when the rpm of the engine was increased was reported by Siller et al. [13]. An interpretation of this result is that when the jet noise is low for low engine power settings, the core noise is a significant contributor to noise in the near field. However, as the jet noise becomes more significant, the coherence drops, due to the relatively low contribution of the combustion noise. This rationale assumes a linear frequency-response function between the combustor can and the exit plane of the engine. It is also possible that the reduction in coherence is due to nonlinear interactions as the unsteady pressure from the combustor passes through the rotor/stator stages. This paper examines the scenario in which a fluctuating pressure is modified in a *nonlinear* sense as it propagates through a rotor/stator stage.

Acoustic interaction between rotors is a common observation in turbomachinery noise measurements and has been discussed analytically by Cumpsty [14], Holste and Neise [15], and Enghardt et al. [16] and numerically by Nallasamy et al. [17]. Energy at two different frequencies may interact to induce energy at a third frequency. In these situations, the upstream energy source is a rotor/stator pair for which the excited spinning modes impinge upon a second rotor. However, the case in which broadband or narrowband noise (which may originate from a combustor) interacts with a rotor/stator pair (e.g., turbine noise), producing noise at sum and difference frequencies, is a relatively unexplored area. Evidence of this phenomenon is presented in the paper and the process is thought to be analogous with the theories reported by Cumpsty [14] and Moore [18] (i.e., acoustic energy from the combustor propagates down the duct as a spinning mode that subsequently interacts with a downstream rotor).

The nonlinear analysis of this paper investigates how to accommodate, in addition to propagated combustion noise and turbine noise measured at the exit plane of an aeroengine, the possibility of an interaction between the upstream combustion noise

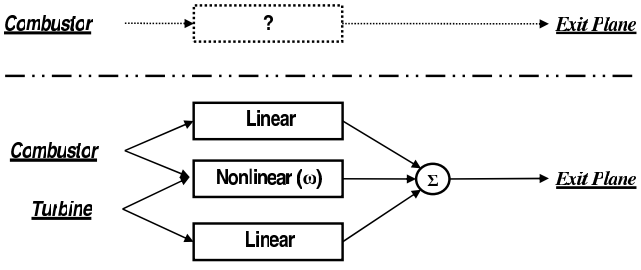

Fig. 2 Frequency-response function between the combustion noise and the pressure measured at the exit plane when some rpm-dependent nonlinearity is included in the model.

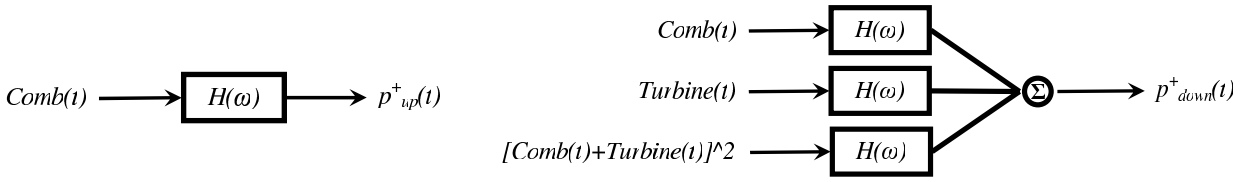

a) Incident pressure upstream, $p^+_{up}(t)$ **b) Incident pressure downstream, $p^+_{down}(t)$**

Fig. 3 Incident pressure models accommodating a quadratic nonlinear term.

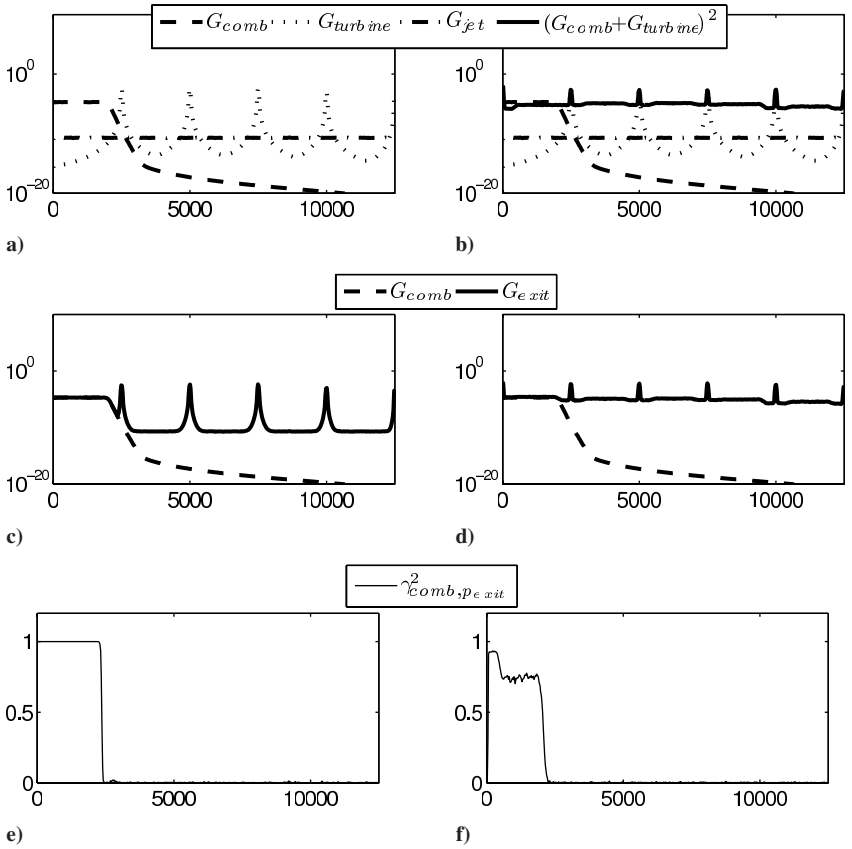

Fig. 4 Combustion-noise, turbine-noise, and jet-noise simulation at a *low* power setting; left column contains a nonlinear quadratic interaction term.

and the turbine, as outlined in Fig. 2. What is suggested is that the additional inputs into the system due to nonlinearities could be an alternative cause for the drop in coherence with increasing engine speed, as measured by Siller et al. [13], and not simply the relative decrease in importance of the combustion noise compared with the other linear terms. As will be seen in the following simulations, quite the opposite could be true. In a nonlinear system, a drop in coherence with increasing engine speed could occur when there is no relative change in power of the linear noise sources. This may lead to the incorrect conclusion that combustion noise is less significant and may, as a result, be ignored in the development of acoustical treatment. It is demonstrated that the effect is similar to a nonlinear quadratic operation being performed on the sum of the two noise sources.

A. Nonlinear Simulations

To investigate the influence of the nonlinear interactions, a series of simulations were performed using synthetic data. A common nonlinear interaction is quadratic in nature, resulting in sum and difference frequencies, as well as a doubling in frequency. This can be demonstrated by observing the following two trigonometric identities:

$$[A\cos(\omega t)]^2 = \tfrac{1}{2}A^2[1+\cos(2\omega t)] \tag{2}$$

$$\begin{aligned}[A\cos(\omega_1 t)+B\cos(\omega_2 t)]^2 &= \tfrac{1}{2}A^2[1+\cos(2\omega_1 t)]\\ &+\tfrac{1}{2}B^2[1+\cos(2\omega_2 t)]+AB\cos(\omega_1+\omega_2)t\\ &+AB\cos(\omega_1-\omega_2)t\end{aligned} \tag{3}$$

The doubling of frequency arises from self-interaction, whereas the sum and difference frequencies come about from combination interactions.

For the simulations of an aeroengine, Fig. 3 shows the input models for upstream and downstream of the turbine, for which it is assumed in this figure that only incident sound is measured. The synthetic data were generated in MATLAB using filtered statistically independent random data signals. Figure 4a shows the basic simulation. This is the *low*-power case; that is, in its frequency range, combustion noise is greater than jet noise. In addition to the linear input terms of Fig. 3 (tonal turbine noise and low-frequency band-limited combustion noise),[‡] the exit-plane measurement of an aeroengine is simulated to contain broadband jet noise. Figure 4b shows the simulated nonlinear quadratic input $(G_{\text{comb}}+G_{\text{turbine}})^2$ in addition to the others. An important point to be noticed here, is that

[‡]Combustion noise is generally limited to a frequency range below 800 Hz and typically peaks in the 200–500-Hz region; however, for reasons of clarity, this range is increased in these figures.

due to the frequency interactions, significant energy is created at frequencies for which the energy of the linear terms is quite low. The middle row of Fig. 4 shows the sum of the exit-plane components, which represents an exit-plane measurement. Also shown is the combustion noise, which represents an upstream measurement. The bottom row plots the coherence between the latter two (i.e., the combustion noise and the total noise). It is shown that for this *low*-power case, the coherence is quite high. For the higher frequencies, the coherence drops off because the contribution of the upstream combustion noise to the exit-plane measurement at these frequencies is negligible.

Figure 5 plots the same information for the *high*-power case. In the left column, all three inputs increase by the same amount, relative to the left column of Fig. 4, which results in no change to the coherence. In the middle column, the turbine noise and combustion noise increase by the same amount as in the left column, but the jet noise increases relatively more. The coherence is seen to drop here, due to the relative decrease in contribution of the combustion noise to the total noise. This is the linear interpretation of the data presented by Siller et al. [13]. The right column shows the same increase in power of the three linear terms as in the left column, but in this case, due to the nonlinear nature of the quadratic term, it increases relatively more, causing it to dominate, which results in the drop in coherence. It is therefore the presence of the nonlinearity that causes the drop in coherence and not a decrease in the combustion noise relative to the other linear terms.

Given the two latter scenarios (namely, 1) three linear terms only, in which the jet noise is relatively higher than the combustion noise in that frequency range and 2) three linear terms, with the combustion noise being highest apart from the nonlinear term in that frequency range), Fig. 6 may now be addressed. From observation of the middle row, the total pressure measured is similar for the two cases (i.e., tonal harmonics with a broadband noise floor). To insert a core liner aft of the turbine in the first scenario will have little effect for this high power case, because the jet noise is dominant and is created beyond the exit plane. In the second case, however, there is a benefit to be gained, because the low-frequency noise is generated upstream of the exit plane and can be attenuated by the liner. Even greater noise attenuation may be attained by reducing the combustion noise (or turbine noise) at the source in the presence of a nonlinear system that couples the two. By eliminating the combustion noise at the source, its contribution will not only disappear from its low-frequency range, but also from higher-interaction frequencies. In the left column of Fig. 6, we see little benefit from eliminating the combustion noise in which jet noise dominates. This figure highlights the benefits to be gained by combustion-noise reduction in the presence of a nonlinear interaction, as well as how important it is to be able to identify the nonlinear process, because incorrect deductions can be made without knowledge of its presence.

A second set of simulations was performed with narrowband noise for the combustor instead of the low-frequency band-limited noise used in the previous simulations. Jet noise is omitted from these simulations to simplify the analysis. It can be seen readily in Fig. 7b that the nonlinear term is made up of double frequencies as well as sum and difference tones.

From Fig. 7, it can be seen that if the COP technique was used between the combustion noise only and the total noise, then the only contribution to the total noise made by the combustor would be identified as being low-frequency narrowband noise. The coherence for this case is shown in Fig. 8a. For a nonlinear process, this would be an incorrect deduction, however, because the combustor also contributes to the total noise at all the higher-interaction frequencies. Without close inspection and measurement, the higher-interaction frequencies could be misinterpreted as rotor/stator interaction noise, particularly for aeroengines with many blades and vanes over many stages.

Figure 8b shows the coherence for the ideal situation for identification of where the upstream contribution of the combustor and turbine only can be measured. For this case, dropouts or a reduction in the coherence are attributable to the additional nonlinear term. When other valid terms are present in the downstream measurement (e.g., jet noise, hydrodynamic noise, or other acoustic linear sources), the coherence in Fig. 8b will also drop. To identify the nonlinear terms more directly, assuming a quadratic interaction, the coherence between the square of the combustor and turbine contributions can be formed in the time domain and the coherence

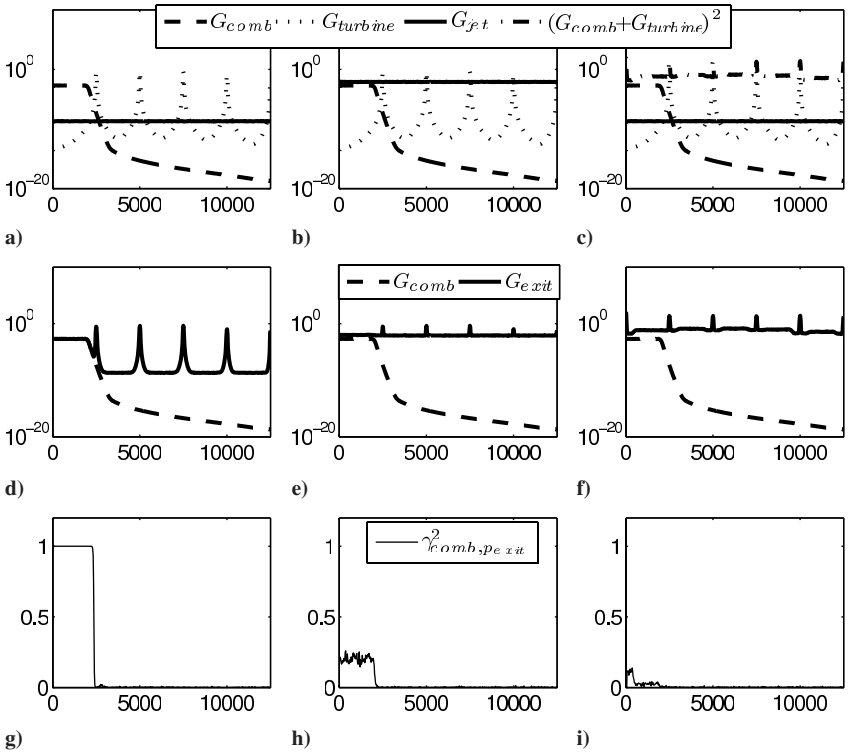

Fig. 5 Combustion-noise, turbine-noise, and jet-noise simulation at a *high* power setting; left column, all three components have been increased by the same amount; middle column, combustion and turbine noise were increased the same amount as the left column, but jet noise was increased by relatively more; right column, linear inputs are increased the same amount as in the left column.

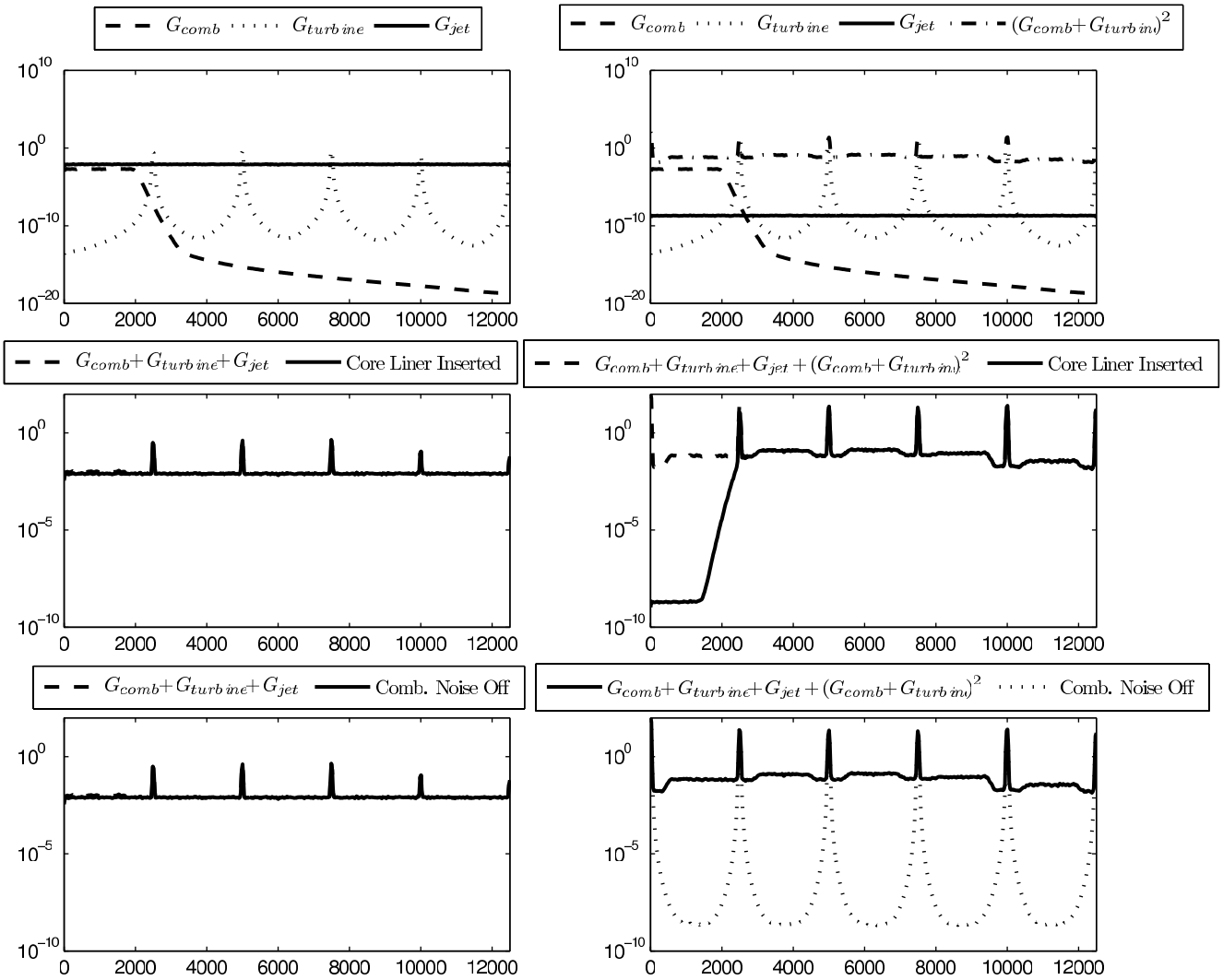

Fig. 6 Comparison of the two scenarios; total exit-plane pressure is similar in both cases (however, in the first case, jet noise dominates, whereas in the second case, it is the nonlinear term that is greatest).

between this and the downstream measurement can be determined, as shown in Fig. 8c.

In practical situations, a measurement of the combustor noise and turbine noise in isolation is not always available in the presence of nonlinear interactions. In this paper, a technique is developed in which the nonlinear contribution is measurable even when the turbine and nonlinear contributions are propagated to the upstream measurement location.

B. Experimental Setup

An experimental rig was designed to examine the propagation of noise through a rotor/stator setup and is shown schematically in Fig. 9. The speaker represents the source noise, which is directed down a brass tube of 3-mm wall thickness with an internal diameter of 0.051 m. This end of the tube is open and allows air to be drawn into the pipe by the vane axial fan situated at a minimum of 1.2 m from the entrance, according to the test setup. This vane axial fan, which has a single eight-blade rotor stage downstream of a single five-vane stator stage represents a simplified turbine of the turbofan engine. The tube end is fitted with an open anechoic termination designed to reduce flow expansion/separation noise as well as reflections. Microphones mounted flush with the inside of the pipe can be located upstream and downstream of the fan at various axial and circumferential positions. Additional microphones can also be located in the near field at the exit plane. Also illustrated is $s(t)$, the electrical signal to the speaker. This signal can be recorded and used to condition the measured pressures, if necessary.

A 32-channel data acquisition system was used to acquire the data. This consisted of 2×16 bit simultaneously sampling Kinetic Systems V200 cards mounted into a National Instruments chassis. A PC running LabView was used via a National Instruments peripheral component interconnect card to acquire the data from the National Instruments multisystem extension interface controller card in the chassis. The spectral estimate parameters are given in Table 1. All data, once acquired into time-domain files by LabView, were subsequently processed using MATLAB.

C. Cylindrical Duct Acoustic Modes

For acoustic propagation in an infinite hard-walled cylindrical duct with superimposed constant mean flow velocity $\mathbf{V}$, the pressure $p = p(r, \theta, x, t)$ in cylindrical coordinates is found as a solution of the homogeneous convective wave equation:

$$\frac{1}{c^2}\frac{\mathrm{D}^2 p}{\mathrm{D}t^2} - \frac{\partial^2 p}{\partial x^2} - \frac{1}{r}\frac{\partial}{\partial r}\left(r\frac{\partial p}{\partial r}\right) - \frac{1}{r^2}\frac{\partial^2 p}{\partial \theta^2} = 0 \tag{4}$$

where the substantive derivative is defined to be

$$\frac{\mathrm{D}}{\mathrm{D}t} = \frac{\partial}{\partial t} + \mathbf{V}\frac{\partial}{\partial x}$$

The general solution to Eq. (4), with or without mean flow, can be expressed as a linear combination of eigenfunctions:

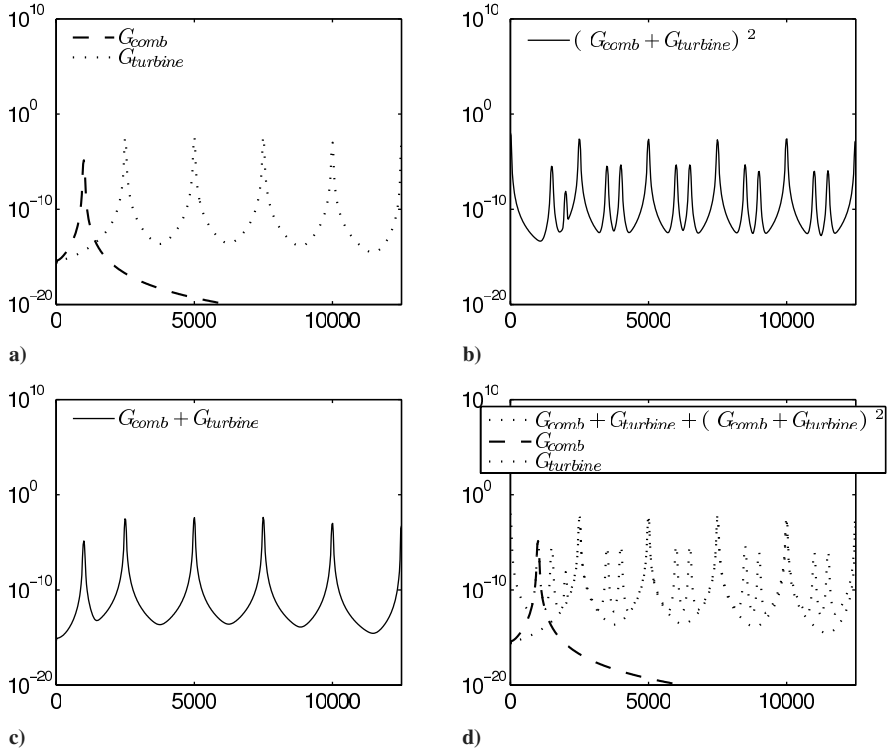

Fig. 7 Narrowband combustion-noise simulation: a) linear sources (combustion noise and turbine noise), b) nonlinear interaction term (if present), c) linear summation of linear sources, and d) downstream measurement when nonlinear interaction has taken place.

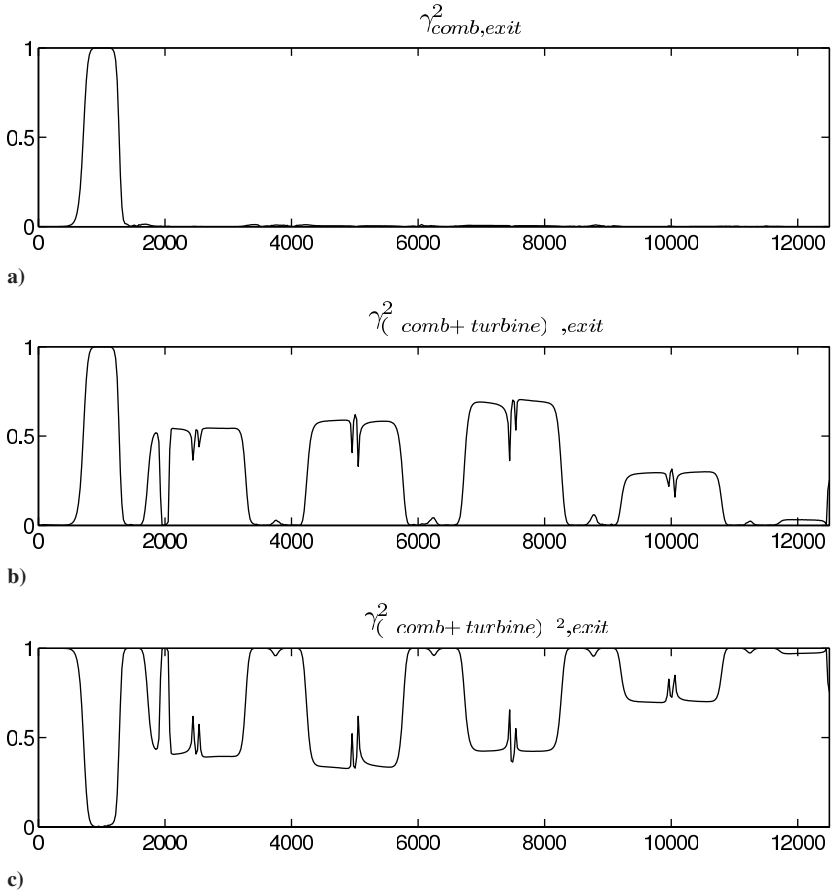

Fig. 8 Coherence function plotted for three different situations: a) between the combustor measurement and the exit-plane measurement, b) between an upstream measurement of the combustor and turbine only noise, and c) between the square of the upstream linear components.

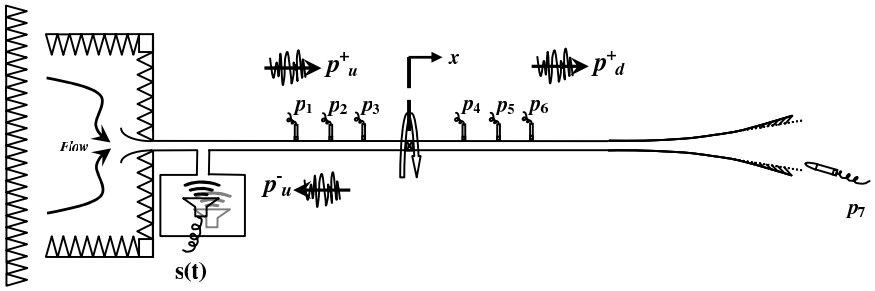

Fig. 9 Schematic of the experimental rig.

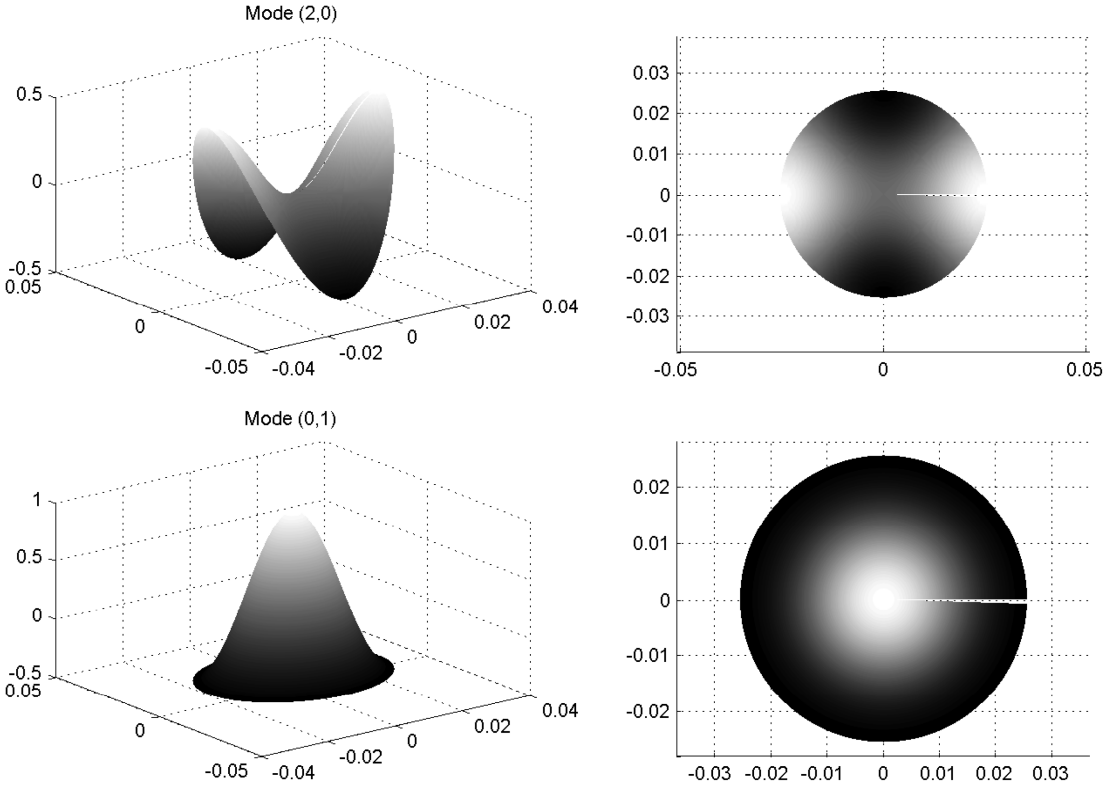

Fig. 10 Acoustic mode shapes (2, 0) and (0, 1).

$$p(r,\theta,x,t) = \mathbf{Re}\left[\sum_{m=0}^{+\infty}\sum_{n=0}^{+\infty} A_{m,n}(x)\Psi_{m,n}(r,\theta)e^{-j\omega t}\right] \qquad (5)$$

where the eigenfunctions $\Psi_{m,n}(r,\theta)$ of amplitude $A_{m,n}(x)$ will depend uniquely on the cross-sectional shape of the duct. For the case of a hard-walled cylindrical duct, the eigenfunction is

$$\Psi_{m,n}(r,\theta) = J_m(k_{r,m,n}r)e^{jm\theta} \qquad (6)$$

An examination of Eq. (5) can be used to discuss the physics of the sound field in the duct. The eigenfunction is a mode shape that may be generated at a frequency ω in the (r,θ) plane perpendicular to the x axis and that may propagate as a traveling wave upstream or downstream in the duct, in accordance with the x-dependent amplitude. The eigenvalues of this equation provide frequencies, cutoff frequencies, above which generated modes propagate unattenuated, but below which excited modes exponentially decay. Several modes may coexist in the duct at a frequency of excitation, as long as this frequency is above their individual cutoff frequencies. The pressure in the duct is assumed to fluctuate harmonically, as can be seen from the exponential time term $e^{(-j\omega t)}$. The transverse eigenvalue of the (m,n)th mode, $k_{r,m,n}$, is also called the transverse, combined radial–circumferential, or simply the radial wave number.

According to Eq. (6), it can be seen that the normal modes are sinusoids in the circumferential direction and Bessel functions in the radial direction, in which m specifies the circumferential mode number and n indicates the associated radial mode number. The (0, 0) mode indicates the plane-wave mode, (1, 0) indicates the first circumferential (or azimuthal) mode, and (0, 1) indicates the first radial mode. Figure 10 gives an example of two mode shapes.

D. Experimental Results

An analysis was performed on the experimental rig of Sec. II.B to detect the presence of nonlinearities. As seen in Fig. 7, tonal interactions are more distinctive than broadband, and so tonal noise was emitted from the speaker when performing the diagnostic. To investigate this hypothesis that upstream noise might interact with a rotor/stator pair to produce acoustic energy at sum and difference frequencies, the experimental investigation had to be extended above the plane-wave frequency region.

While varying the amplitude and frequency of the speaker signal, the power spectral density (PSD) of a microphone located downstream of the fan was examined. A set of tests was carried out in which the speaker tone was incremented in steps of 500 or 250 Hz, from 500 Hz to 12.5 kHz. A waterfall plot of these results is shown in Fig. 11. The first averaged PSD in this plot is only for the fan turned on. The fan has a high rotational speed of 16,500 rpm at the nominal

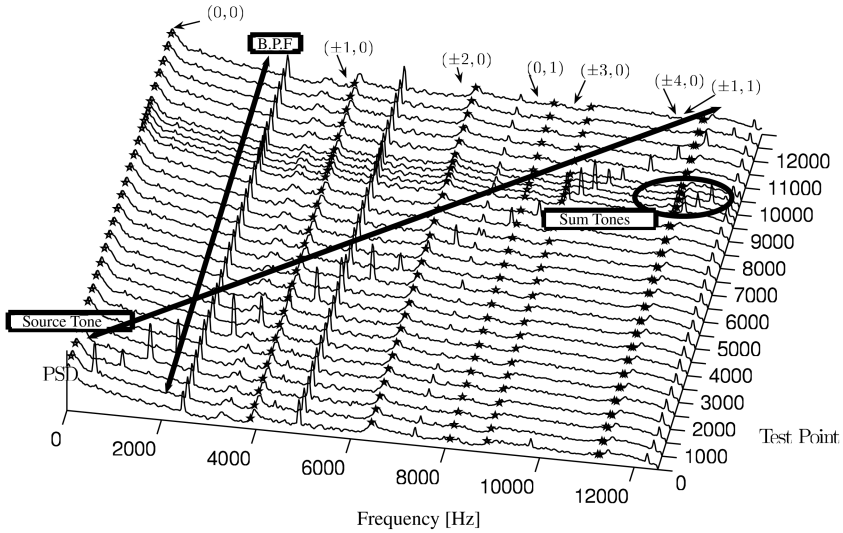

Fig. 11 For microphone 5 only, the results of the investigation with and without the vane axial fan turned on.

maximum design voltage of 26-Vdc. Because the fan has eight blades, this results in a blade pass frequency (BPF) of 2200 Hz, a peak that can be seen in Fig. 11, along with its harmonics nBPF, four of which are visible up to the Nyquist frequency.

With each successive test, the frequency from the speaker is increased. This plot is revealing because there is no indication of nonlinear interaction until the speaker frequency reaches 8.75 kHz, above which only a sum tone with the BPF is detectable; for example, a sum tone at 10.95 kHz is visible, which is the result of the addition of the BPF (2.2 kHz) and the speaker tone (8.75 kHz). Similar sum tones are to be seen in Fig. 11 as the speaker tone increases in frequency. In addition to sum frequencies, if the model of Fig. 3b (i.e., a quadratic model) is to be respected, difference frequencies between the speaker tone and the BPF and its harmonics should also be measurable;for example, a difference tone at

$$2400 \text{ Hz (BPF)} - 500 \text{ Hz (speaker)} = 1900 \text{ Hz}$$

should be present in Fig. 11. Figure 12 plots, as an example, the expected interactions for an upstream speaker tone of 9.3 kHz with the nBPF frequencies assuming a quadratic model. The lowest difference tone to be seen is at

$$300 \text{ Hz} = 9600 \text{ Hz } (4 \times \text{BPF}) - 9300 \text{ Hz (speaker)}$$

for example. To help understand why there is a disparity between the interaction frequencies measured in Fig. 11 and those expected, the cutoff frequencies for the higher modes in the duct were calculated. These values are given in Table 2 for this diameter duct and the relevant values are superimposed onto the waterfall plot (black stars). It can be seen clearly that the interaction tone appears only above $\approx 11,200$ Hz, which is either the $(\pm 4, 0)$ cutoff frequency or the $(\pm 1, 1)$ cutoff frequency. It was therefore posited that the interaction tone has a modal structure of either $(+4, 0)$, $(-4, 0)$, $(+1, 1)$, or $(-1, 1)$ or possibly some combination of these. In addition, it is

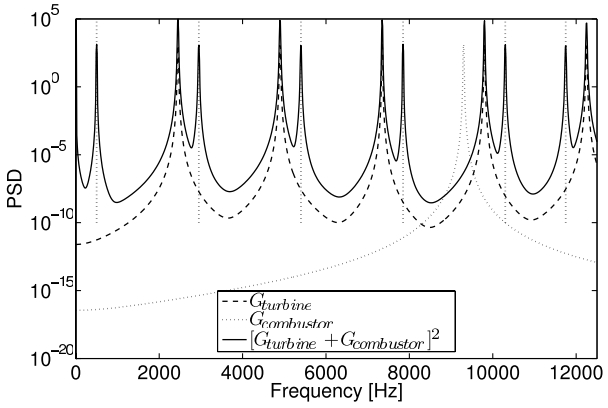

Fig. 12 Simulated data representing a quadratic interaction between the turbine and combustor, with a BPF of 2400 Hz and a combustor frequency of 9.3 kHz.

Table 1 Spectral estimate parameters: experimental rig

Parameter	Value
Segment length (data points per segment) Np	1024
Sample rate f_{samp}, samples per second	25,000
Segment length $T_d = Np/f_{\text{samp}}$, s	0.04096
Sampling interval $\Delta t = 1/f_{\text{samp}}$, s	4×10^{-5}
Frequency step $\Delta f = 1/T_d$, Hz	24.41
Upper-frequency limit $f_c = 1/(2\Delta t) = f_{\text{samp}}/2$, Hz	12,500
No. of frequencies $Ly = f_c/\Delta f = Np/2$	512
No. of independent samples	200
Overlap	0
Sample length, s	8.192

Table 2 Cutoff frequencies $f_{m,n}^{\text{cut-off}}$ (in hertz) for 0.05115-m-diam cylindrical duct; $c = 340$ m/s and $M = 0.035$

m, n	0	1	2	3	4	5
0	0	8102	14,835	21,512	28,174	34,827
±1	3893	11,273	18,050	24,753	31,430	38,104
±2	6458	14,180	21,081	27,849	34,568	41,255
± 3	8884	16,959	23,991	30,842	37,615	44,342
±4	11,244	19,628	26,816	33,757	40,591	47,366
±5	13,566	22,245	29,577	36,609	43,508	50,326

Table 3 Spectral estimate parameters: full-scale tests

Parameter	Value
Segment length (data points per segment) Np	8192
Sample rate f_{samp}, samples/s	32,768
Segment length $T_d = Np/f_{\text{samp}}$, s	0.25
Sampling interval $\Delta t = 1/f_{\text{samp}}$, s	3.0518×10^{-5}
Frequency step $\Delta f = 1/T_d$, Hz	4
Upper-frequency limit $f_c = 1/(2\Delta t) = f_{\text{samp}}/2$, Hz	16,384
No. of frequencies $Ly = f_c/\Delta f = Np/2$	4096
No. of independent samples	400
Overlap	0.75
Sample length, s	100

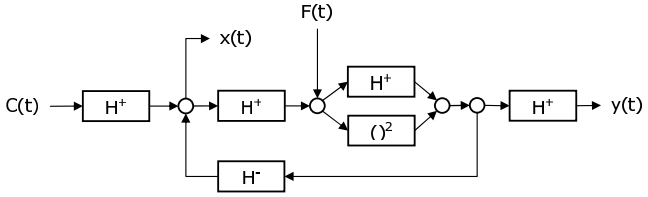

Fig. 13 Actual schematic for upstream and downstream measurements; fan noise and interaction noise is propagated upstream to upstream measurement position.

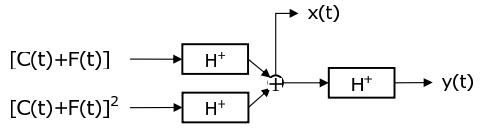

Fig. 14 Inputs into upstream and downstream measurements can be modeled as having linear and nonlinear part; input/output model for nonlinear decomposition.

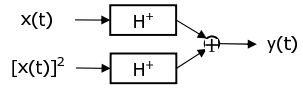

Fig. 15 Input/output model for nonlinear decomposition.

suggested that this modal structure comes about as a result of the interaction of the modal structure of the BPF frequency with that of the speaker frequency. A modal decomposition of the pressure field upstream and downstream of the fan was performed by Bennett [19] that showed the modal content of the interaction tone downstream of the fan to be of the form $(+4, 0)$. It therefore seems likely that the nonlinear term

$$[\text{comb}(t) + \text{turbine}(t)]^2$$

plotted in Fig. 12, needs to be used in conjunction with the duct modal theory. That is to say, if energy at two frequencies interact to create energy at a third, then this energy will only propagate down the duct if the mode that carries it is above its cutoff frequency.

E. Nonlinear Identification Techniques

From the simulations of Sec. II.A, identification of the nonlinear contribution to a measurement downstream of either the vane axial fan of the small-scale experiment or a turbine of an aeroengine should be quite straightforward. Measurements of the individual linear contributions (the combustion noise and the turbine noise) could be added and squared in the time domain and this input could be conditioned from the downstream measurement. Unfortunately, with regard to the rig, although an isolated measurement of the speaker noise is possible indirectly, via the electrical supply signal to the speaker, no means of measuring the vane axial fan noise alone is readily available. The model of Fig. 13 represents the physical situation in the duct. In the figure, the two principle acoustic inputs into the duct are the combustion (speaker) noise and the vane axial turbine (vane axial fan) noise. An upstream measurement is denoted by $x(t)$, whereas $y(t)$ indicates a measurement downstream of the fan. The downstream measurement $y(t)$ will always contain the sum of the linear parts in addition to the nonlinear component, when present, whereas the upstream measurement $x(t)$ will be composed of the source noise as well as the fan noise and the nonlinear contribution (when present), depending on the conditions for back propagation. As a consequence of this, the model of Fig. 13 can be simplified to Fig. 14, in which the second, nonlinear, component is included when the physics dictates. An example can be given with reference to Fig. 11, in which the downstream measurement, in this case, is linear until the speaker signal is raised above 8.75 kHz, above which the second, nonlinear, term needs to be included. The difficulty, therefore, is to separate the nonlinear part from the linear part when the nonlinear part is present.

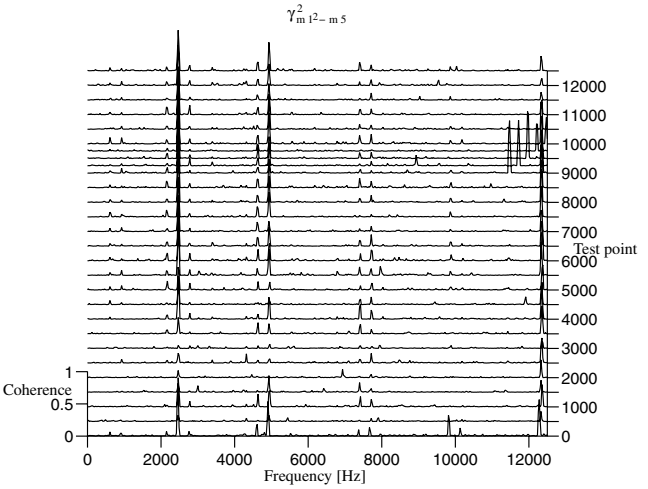

Fig. 16 Coherence between the square of an upstream measurement M1 with a downstream signal M5, calculated for the same test points as those in Fig. 11.

The model presented in Fig. 15 facilitates this linear/nonlinear decomposition when the underlying nonlinear phenomenon is quadratic in nature. Squaring the input $x(t)$ results in the following expansion:

$$((C+F)+(C+F)^2)^2 = \underline{C^2 + 2CF + F^2} + 6C^2F + 6CF^2 + 4C^3F + 6C^2F^2 + 4CF^3 + 2C^3 + 2F^3 + C^4 + F^4 \quad (7)$$

when the nonlinear component is present. As can be seen from the right-hand-side, the first three terms are the expansion of the nonlinear part, whereas the linear parts (i.e., C and F) do not appear. Therefore, a coherence between the square of the input with the output should isolate the nonlinear part of the output only. This technique was applied to the data presented in Sec. II.D, and the result is shown in Fig. 16. As can be seen, the coherence is ≈ 0 apart from at the interaction tones above 11,200 Hz and at some of the nBPF frequencies. In addition, some nonlinear interaction is seen to take place between the shaft imbalance and the nBPF frequencies, with some sum and difference frequencies around the nBPF frequencies identified. The shaft imbalance

$$\frac{\text{BPF}}{\text{no. of blades}} = 2200/8 = 275 \text{ Hz}$$

is nonacoustic, and thus these peaks, along with the nBPF peaks appearing in Fig. 16, are thought to be present as a result of the microphone's sensitivity to vibration.

With reference to Fig. 15, Fig. 16 shows that the nonlinear contribution to the downstream measurement may be isolated by examining the coherence between the square of the upstream measurement and the downstream measurement. To isolate the linear contribution (in the presence of nonlinear interactions), partial coherence techniques, as discussed by Bendat and Piersol [12] and employed by Rice and Fitzpatrick [20], may be used.

Pertinent to this problem are results in which it is calculated that if two arbitrary signals i and j are composed of at least two components each, in which r is one of them, then the cross spectrum between i and j with the linear effects of r removed can be expressed as

$$G_{ij\cdot r} = G_{ij} - \frac{G_{ir}G_{rj}}{G_{rr}} \quad (8)$$

It can be seen from this equation that the part correlated with r must then be

$$G_{ij:r} = \frac{G_{ir}G_{rj}}{G_{rr}} \quad (9)$$

For $i = j$, the autospectrum of either i or j with the linear part of r removed can be written as

$$G_{ii\cdot r} = G_{ii} - \frac{G_{ir}G_{ri}}{G_{rr}} \tag{10}$$

with the correlated part given by

$$G_{ii:r} = \frac{|G_{ri}|^2}{G_{rr}} \tag{11}$$

The *partial coherence function* between i and j with the linear effects of r removed, as derived by Bendat and Piersol [12], may now be defined as the ordinary coherence function between the conditioned spectra:

$$\gamma^2_{ij\cdot r} = \frac{|G_{ij\cdot r}|^2}{G_{ii\cdot r}G_{jj\cdot r}} \tag{12}$$

In summary, for the arbitrary signals i and j, the nonlinear and linear contributions to the coherence function can be given as follows:

Nonlinear coherence:

$$\gamma^2_{(i^2,j)} \tag{13}$$

Linear coherence:

$$\gamma^2_{(i,j)\cdot i^2} \tag{14}$$

III. Full-Scale Engine Tests

A. Introduction

The nonlinear identification techniques developed with the experimental rig were applied to data from full-scale turbofan engine tests. A Rolls-Royce engine was instrumented with pressure transducers at the combustor can and in the hot-jet pipe, and microphones were placed in the near field. A schematic of some of the instrumentation is shown in Fig. 17, and the spectral estimate parameters are given in Table 3. RP1 was located in the combustor outer casing and RP3 was located within the combustor. RP1 and the hot-jet sensor RPB were flush-mounted, and RP3 was positioned at the outer end of an igniter tube to avoid the high temperatures within the combustor. The sensors were manufactured by Vibro-meter and have been proven to have high-frequency and high-temperature capabilities. Microphone 5 (M5) was located 10.04 m from the jet axis and hence clear of the hydrodynamic turbulent pressure fluctuations of the jet. The results from five steady-state points (engine power settings) were examined. The power settings defined for the test included some diagnostic conditions that are not necessarily representative of operational conditions.

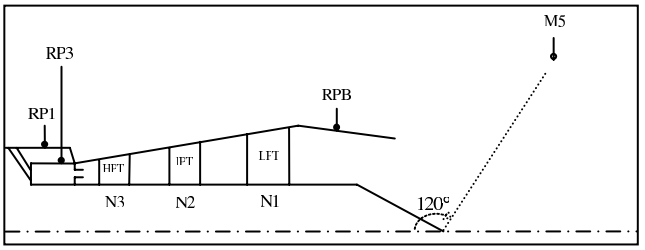

Fig. 17 Engine instrumentation schematic with the location of the external far-field microphone.

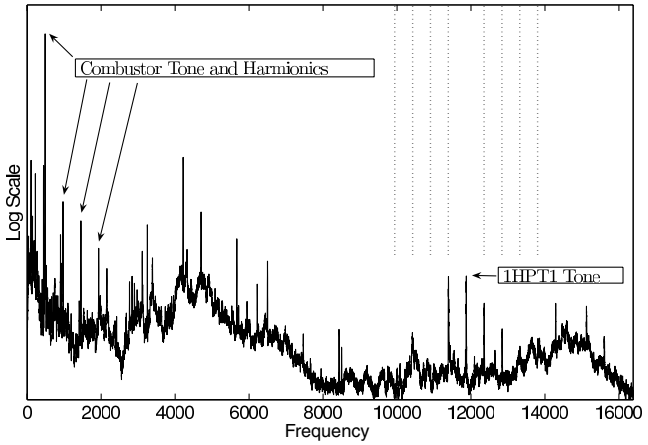

Fig. 18 PSD at the sensor location in the hot-jet pipe RPB for a particular engine power; a combustor tone at ≈500 Hz is measured, as well as the superharmonics; a HPT tone propagated through the turbine is also measured; on either side of this tone is the energy at the sum and difference frequencies.

For the highest of the five test points, the PSD of the hot-jet-pipe transducer RPB is shown in Fig. 18. A number of interesting points can be noted in this figure. First, a tone in the combustor can is generated at ≈500 Hz. This tone is of sufficiently high amplitude to generate superharmonics. The tone and the superharmonics are measurable downstream of the turbine. Second, a tone generated from rotor/stator interaction in the high-pressure turbine (HPT) is measurable downstream of the low-pressure turbine near the exit plane. Third, the combustion tone and its superharmonics interact with this HPT tone in a nonlinear fashion similar to that observed with the experimental rig: sum and difference frequencies are formed due to combustion noise impinging on a rotor/stator pair. It is most significant that not only does this interaction occur, but that the interaction tones, along with the HPT tone and the combustor tones, are able to propagate through the circuitous path created by the various stages of the turbines.

B. Nonlinear Analysis

Typically, as previously discussed, the coherence function is used to investigate, in a causal way, the relationship between combustion noise and a downstream measurement. A waterfall plot is presented in Fig. 19 of the coherence function between the combustion-can sensor RP1 and the hot-jet-pipe sensor RPB for the five test points. The plot is annotated to highlight the HPT tone, which is measured at all test points, and the combustor tone and harmonics, in addition to the sum and difference frequencies, which are measured at the highest point only. Only careful scrutiny and knowledge of rotor vane numbers would allow these peaks to be identified from the many tones to be found in a near-field aeroengine spectrum. Figure 20 shows the same waterfall plot, but in this case, the coherence was calculated between the square of the combustor-can measurement and that of the hot-jet-pipe sensor. It is immediately

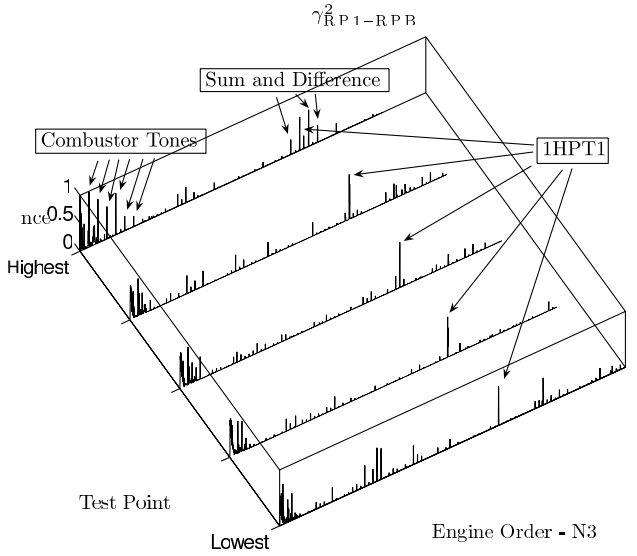

Fig. 19 Coherence between the combustion-can sensor RP1 and the hot-jet-pipe sensor RPB for five increasing-power test points.

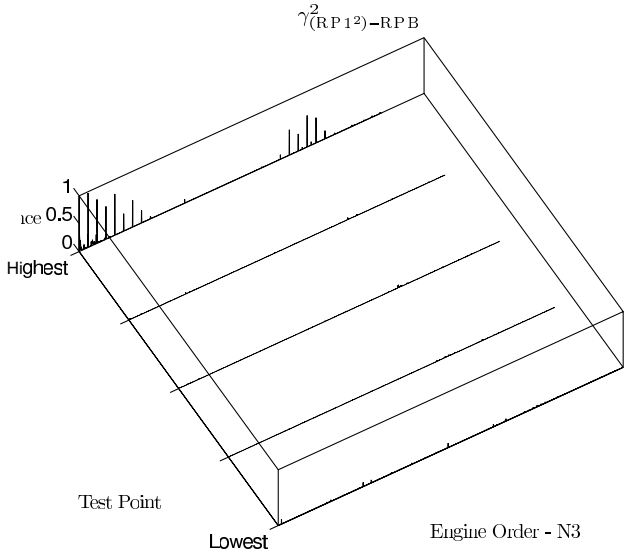

Fig. 20 Coherence between the square of the combustion-can sensor RP1 and the hot-jet-pipe sensor RPB for five increasing power test points; nonlinear interaction is seen to be present only at the highest test point.

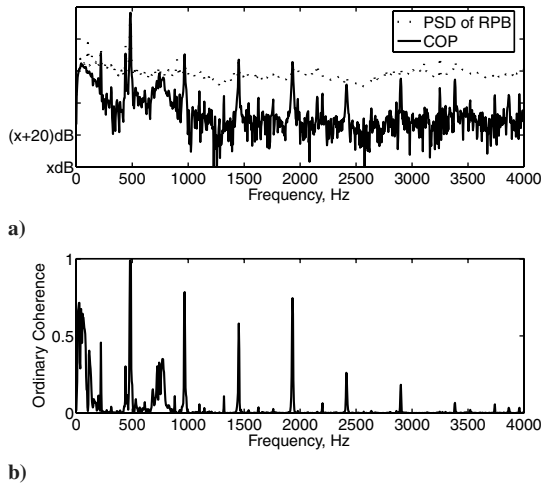

Fig. 21 Linear analysis of a) PSD of RPB compared with the coherent output power using the b) coherence between the combustion-can sensor RP1 and the hot-jet-pipe sensor RPB; only the frequency range 0–4 kHz is displayed.

evident from this plot that nonlinear interaction has taken place at the higher test point and that peaks would be expected in the spectrum that would not be the result of linear noise-source superposition.

In addition to being a tool for nonlinear interaction identification, this quadratic analysis approach can be used, as explained in Sec. II.E, to separate the nonlinear contribution to the spectrum from the linear contribution. The model of Fig. 15 was used and the full-scale test data was processed with the following equations:

Nonlinear COP:

$$\gamma^2_{(RP1^2,RPB)} G_{(RPB,RPB)} \tag{15}$$

Linear COP:

$$\gamma^2_{(RP1,RPB)\cdot RP1^2} G_{(RPB,RPB)\cdot RP1^2} \tag{16}$$

Figure 21 shows the standard COP calculated between the combustor-can location and the hot-jet-pipe location. This coherence function of Fig. 21b, in conjunction with the COP in Fig. 21a, would be used, for example, to assess the frequency range for which acoustic treatment might be designed to reduce combustion-noise

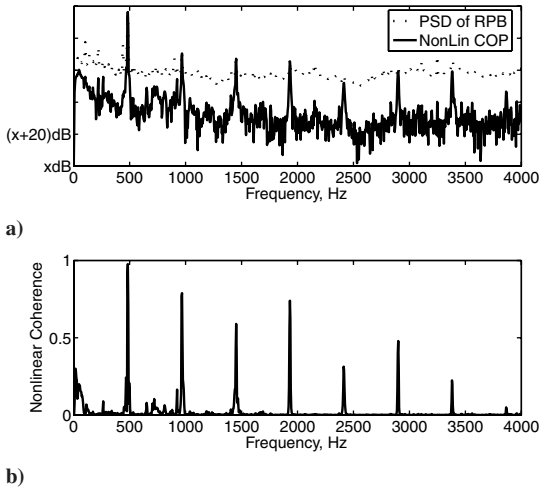

Fig. 22 Nonlinear part of the COP vs the PSD of RPB and the linear part of the COP vs the PSD of RPB.

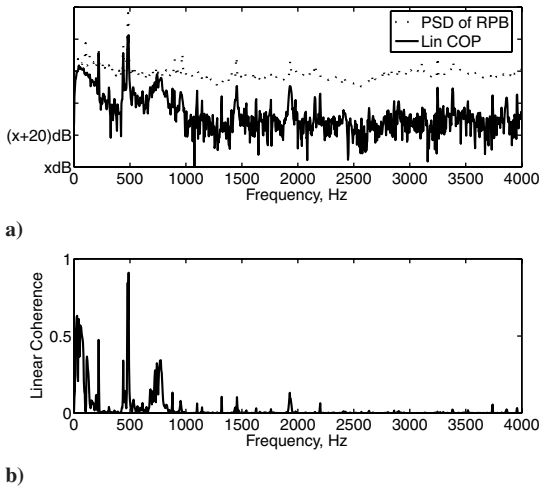

Fig. 23 Linear part of the COP vs the PSD of RPB.

radiation to the far field. However, as Fig. 22 displays, the frequency range that the nonlinear contribution spans is far greater than that attributable to the actual sound source, as plotted in Fig. 23. Because it is difficult to design acoustic treatment to absorb sound over a large frequency range, the ability to identify the nonlinear contribution means that efforts can be divided into two parts: 1) absorption or reduction of the (linear) combustion noise, ideally, upstream of the turbine and 2) tackling the nonlinear interaction process separately. Obviously, if the combustion noise is reduced upstream of the turbine, then, as highlighted in the simulations, the contribution of the nonlinear noise is greatly diminished.

This analysis was also applied to the frequency range around the 1HPT1 tone and successfully identified the sum and difference tones and subtracted them from the COP, decomposing it into linear and nonlinear parts.

IV. Conclusions

In this paper, the ability for coherence-based noise-source identification techniques to identify core noise in aeroengines was discussed. An experimental rig was designed and built to gain a fundamental physical understanding of the propagation of noise through a rotor/stator setup. Experiments performed on the rig allowed it to be shown experimentally that acoustic energy in a duct at a certain frequency may interact with rotor/stator noise at a different frequency to scatter energy to a third frequency that is a sum of the two. The case in which broadband or narrowband noise (which

may originate from a combustor, as opposed to an upstream rotor) interacts with a rotor/stator pair (e.g., turbine noise), producing noise at sum and difference frequencies, was explored in this paper. An experimental technique was developed that enables the nonlinear interaction between the propagated sound source with the vane axial fan to be detected and identified when present. The technique was extended to allow the linear and nonlinear acoustic contributions to be separated. From analysis of data from full-scale turbofan engine tests, scattering was seen to occur between the combustion noise and the high-pressure turbine, which was measurable in the hot-jet pipe after propagation through the many turbine stages. The techniques allowed the nonlinear interaction to be successfully identified and linear and nonlinear coherent output powers to be determined.

Acknowledgment

This work was partly supported by the SILENCE(R) project, which is funded under European Union Commission contract no. G4RD-CT-2001-00500.

References

[1] Karchmer, A. M., and Reshotko, M., "Core Noise Source Diagnostics on a Turbofan Engine Using Correlation and Coherence Techniques," NASA TM X-73535, 1976.

[2] Karchmer, A. M., Reshotko, M., and Montegani, F. J., "Measurement of Far Field Combustion Noise from a Turbofan Engine Using Coherence Function," 4th AIAA Aeroacoustics Conference, Atlanta, GA, AIAA Paper 77-1277, Oct. 1977.

[3] Reshotko, M., and Karchmer, A. M., "Core Noise Measurements from a Small General Aviation Turbofan Engine," NASA TM81610, 1980.

[4] Halvorsen, W. G., and Bendat, J. S., "Noise Source Identification Using Coherent Output Power Spectra," *Sound and Vibration*, Vol. 9, No. 8, 1975, pp. 15, 18–24.

[5] Karchmer, A. M., "Conditioned Pressure Spectra and Coherence Measurements in the Core of a Turbofan Engine," NASA TM82688, 1981; also AIAA Paper 81-2052, 1981.

[6] Shivashankara, B. N., "High Bypass Ratio Engine Noise Component Separation by Coherence Technique," *Journal of Aircraft*, Vol. 20, No. 3, 1983, pp. 236–242.

[7] Shivashankara, B. N., "High Bypass Ratio Engine Noise Component Separation by Coherence Technique," *Journal of Aircraft*, Vol. 23, No. 10, 1986, pp. 763–767.

[8] Chung, J. Y., "Rejection of Flow Noise Using a Coherence Function Method," *Journal of the Acoustical Society of America*, Vol. 62, No. 2, 1977, pp. 388–395.

[9] Hsu, J. S., and Ahuja, K. K., "A Coherence-Based Technique to Separate Ejector Internal Mixing Noise from Far-Field Measurements," 4th AIAA/CEAS Aeroacoustics Conference, AIAA Paper 98-2296, June 1998.

[10] Minami, T., and Ahuja, K. K., "Five-Microphone Method for Separating Two Different Correlated Noise Sources from Far-Field Measurements Contaminated by Extraneous Noise," 9th AIAA/CEAS Aeroacoustics Conference, AIAA Paper 03-3261, May 2003.

[11] Bennett, G. J., and Fitzpatrick, J. A., "A Comparison of Coherence-Based Acoustic Source Identification Techniques," International Congress on Sound and Vibration Paper 950, July 2005.

[12] Bendat, J. S., and Piersol, A. G., *Random Data: Analysis and Measurement Procedures*, Wiley, New York, 1986.

[13] Siller, H. A., Arnold, F., and Michel, U., "Investigation of Aero-Engine Core-Noise Using a Phased Microphone Array," 7th AIAA/CEAS Aeroacoustics Conference, Maastricht, The Netherlands, AIAA Paper 2001-2269, May 2001.

[14] Cumpsty, N. A., "Sum and Difference Tones from Turbomachines," *Journal of Sound and Vibration*, Vol. 32, No. 3, 1974, pp. 383–386. doi:10.1016/S0022-460X(74)80094-5

[15] Holste, F., and Neise, W., "Noise Source Identification in a Propfan Model by Means of Acoustical Near Field Measurements," *Journal of Sound and Vibration*, Vol. 203, No. 4, 1997, pp. 641–665. doi:10.1006/jsvi.1996.0890

[16] Enghardt, L., Tapken, U., Neise, W., Kennepohl, F., and Heinig, K., "Turbine Blade/Vane Interaction Noise: Acoustic Mode Analysis Using In-Duct Sensor Rakes," 7th AIAA/CEAS Conference on Aeroacoustics, Maastrict, The Netherlands, AIAA Paper 2001-2153, May 2001.

[17] Nallasamy, M., Hixon, R., Sawyer, S., Dyson, R., and Koch, L., "A Time Domain Analysis of Gust-Cascade Interaction Noise," 9th AIAA/CEAS Aeroacoustics Conference and Exhibit, Hilton Head, SC, AIAA Paper 2003-3134, May 2003.

[18] Moore, C. J., "In-Duct Investigation Of Subsonic Fan 'Rotor-Alone' Noise," *Journal of the Acoustical Society of America*, Vol. 51, No. 5A, 1972, pp. 1471–1482. doi:10.1121/1.1912997

[19] Bennett, G. J., "Noise Source Identification for Ducted Fans," Ph.D. Thesis, Trinity College Dublin, Dublin, Northern Ireland, U.K., 2006.

[20] Rice, H. J., and Fitzpatrick, J. A., "A Generalised Technique for Spectral Analysis of Nonlinear Systems," *Mechanical Systems and Signal Processing*, Vol. 2, No. 2, 1988, pp. 195–207. doi:10.1016/0888-3270(88)90043-X

D. Gaitonde
Associate Editor